Landsat-based long–term LUCC mapping in Xinlicheng Reservoir Basin using object-based classification

Wei Su[1,*], Dongmei Liang[1], Gula Tang[2], Zundong Xiao[1], Jingxin Li[1], Zhengyu Wan[1] and Ping Li[1]

[1]Jilin Provincial Academy of Environmental Sciences, Changchun 130012, China
[2]Key Laboratory of Agricultural Remote Sensing, Ministry of Agriculture/Institute of Agricultural Resources and Regional Planning, Chinese Academy of Agricultural Sciences, Beijing 100081, China

*Corresponding author e-mail: suwei.e@foxmail.com

Abstract. Rapid urbanization dramatically changes the local environment around Xinlicheng Reservoir Basin. Landsat images are suitable for the land use change caused by human impact. In order to obtain consistent land cover products, a hybrid classification method combining object-based classification and pre-classification alteration detection method was developed and applied to long-term multi-temporal Landsat images to obtain land cover change information. Object-based classification method was combined with Random forest (RF) classifier to classify the Landsat image in 2008. Then the changed areas in 2000, 2004, 2012, and 2016 were identified by comparing with the images in 2008 via the re–weighted multivariate alteration detection transformation method. The images in 2000, 2004, 2012 and 2016 were classified by RF classifier. Land cover maps for 2000, 2004, 2012, and 2016 were produced by combining the unchanged area in 2008 with the new classes of the changed areas in 2000, 2004, 2012 and 2016. According to the accuracy assessment, the overall accuracy of the land covers of the four periods are all greater than 93%. The accuracy assessment indicates that this hybrid method can produce consistent land cover datasets for a long time period.

1. Introduction

Land use / land cover change (LUCC) is an important part of global climate change and global environmental change research [1]. LUCC is the most direct signal that expresses the influence of human activities on the natural ecological system of land surface. LUCC is the link between human social and economic behavior and natural ecological process. LUCC have an important impact on the regional ecological environment, and affect global environmental change in a cumulative manner [2-4]. It is generally believed that natural conditions and anthropogenic activities are important drivers of LUCC, which together affect the manner and intensity of LUCC. LUCC has become a hot topic at science research.

Traditionally, most LUCC identifications involve time-consuming and laborious field surveys. In recent years, with the development of remote sensing technology, a growing number of studies have

focused on utilizing satellite data to detect the phenology of different land use types because the frequent remotely sensed images have significant potential for monitoring LUCC dynamics [5-7].

Currently, the methods based on pixels ignore the useful context information, thus leading to "salt and pepper" effects on the classification result [8]. On the contrary, object-based classification methods are currently gaining more attentions [9, 10]. Compared with a pixel, an object is a group of homogeneous pixels that represent a meaningful object in the real world, and contains richer information regarding the shape, context and spatial relationship of the object. To retrieve information from these images, geographic object-based image analysis has been widely used and represents an evolving paradigm [11, 12]. The object-based methods are less sensitive to registration errors and can effectively solve the "salt and pepper" effect. The spatial features can significantly improve the classification performance. More advanced methods for object identification, referred to as Object Based Image Analyses (OBIA), have been developed and applied to e.g. land-use classification where they have provided substantial improvement [13, 14]. This class of techniques builds on segmentation, edge-detection, feature extraction and classification concepts that are combined to improve the performance.

Xinlicheng Reservoir Basin is an important ecological barrier and an important water source in Changchun City. The water quality of Xinlicheng Reservoi has become a problem related to resident health and national economic development. The monitoring and evaluation of reservoir water quality has always been a relatively important research areas. With the continuous expansion of Changchun city scale, the population has increased dramatically, and the problem of urban drinking water supply has been paid more and more attention by all sectors of society. With the development of urbanization, the structure and function of land use in Xinlicheng Reservoir Basin changed drastically. The land use change will inevitably lead to the change of structure, type and regional configuration of vegetation cover, and then the stability and equilibrium of the basin ecosystem have a far-reaching impact. In addition, the existence of salinization in the region seriously restricts the development of local and its surrounding areas. At present, the study of this basin is focused on water quality and pollutants, and there is little research on long-term high-resolution land use.

In the study, the combination of the object-based classification method and IR-MAD change detection method were used to classify the Landsat satellite data from 2000 to 2016 to provide the high-resolution and long-term LUCC dataset [15, 16]. Based on the analysis of the results, the LUCC characteristics of the Xinlicheng Reservoir Basin are presented, and the LUCC can provide the basis to support the environment protection and rational utilization of land.

2. Study area and data pre-process

2.1. Study area

Xinlicheng Reservoir Basin lies in the middle of Jilin province, south of Changchun City. The outlet of the Xinlicheng Reservoir Basin is 16km away from Changchun City. The area covered by Xinlicheng Reservoir Basin is between northern latitude 43°3′~43°44′ and eastern longitude 125°0′~125°37′. The area of Xinlicheng Reservoir Basin is 1970 km^2. Xinlicheng Reservoir is located at the end of the Xinlicheng River Basin. Xinlicheng Reservoir is a large reservoir that is equipped with a comprehensive river channel for water supply, flood control, irrigation and tourism in Changchun City. Xinlicheng Reservoir east-west width of 15-30 m, north-south extension of 16 km, is a shallow lake. The study area is located in the temperate continental monsoon climate zone. In Xinlicheng reservoir Basin, the main rivers include Yitong River, Yidan River, Nadanbo River, Jiaguan River, Xinxing River, which are all seasonal rivers. Yidan River and Nadanbo River are the main upstream rivers of the Xinlicheng Reservoir.

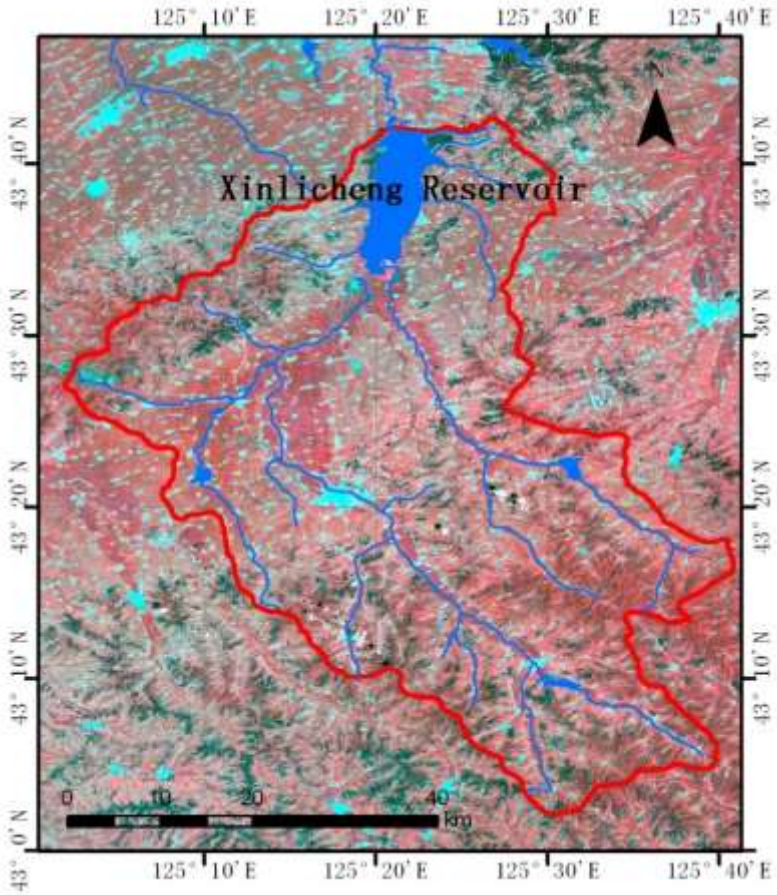

Figure 1. The study area.

2.2. Data preprocess

2.2.1. Classification system and sampling. Taking into account the spatial resolution of Landsat images and application requirements, the classification system includes 7 categories of existing classification systems: forest, grass, dry farmland, paddy field, bare land, building, and water body. The training samples were collected primarily through a visual interpretation Landsat images in 2008 referring to Google Earth. The sample points are randomly distributed in the study area.

2.2.2. Landsat images reprocessing. The land use change caused by human impact is limited, which is far lower than that caused by climate change and natural disasters. In China, this limitation is more obvious due to the small-scale individual-owned farmland (usually smaller than 1 ha). Therefore Landsat images with 30m resolution are particularly important [5]. The Landsat satellite series has continually observed Earth since 1972 and has accumulated an enormous number of time series images [17]. Landsat images have been widely used in land-cover classification because of their stable imaging quality [5, 18-21]. In this study, Level 1 terrain corrected (L1T) Landsat images were selected as the primary data source for the land-cover classifications. The Landsat images were atmospherically corrected to produce the surface reflectance by using the Landsat Ecosystem Disturbance Adaptive Processing System.

Table 1. The acquired Landsat images.

Date	path/row	Sensor
2000/09/26	118/30	Landsat 5
2004/09/21	118/30	Landsat 5
2008/09/16	118/30	Landsat 5
2011/06/05	118/30	Landsat 5
2016/09/22	118/30	Landsat 8

The acquired Landsat images were shown in table 1. However, in study area, there was not acquired Landsat image in 2012. In order to accomplish the land over every 4 years, the STARFM was used to predict the Landsat 5 image acquired on September 16, 2012 [22]. Therefore the MODIS daily surface reflectance (MOD09GA) data in June 5, 2011 and September 16, 2012 were re-projected and resampled to Landsat resolution and extend. Finally, the STARFM produced the predicted Landsat5 images in September 16, 2012.

3. Methods

The Object-oriented classification method was used in this study. First, random forest classifier was used to classify the Landsat 5 images in 2008 and then the land cover of 2008 was produced. In order to obtain consistent land cover products, the pre-classification method was used to detect the changed area. In the specific operation, the Landsat 5 image in 2008 was used as the reference image, and the IR-MAD method was used to detect the change area of the Landsat images in 2000, 2004, 2012 and 2016 compared with the Landsat 5 image in 2008. After detecting the changed areas, the random forest classifier was used to classify the changed areas. The land covers of the changed area were then integrated with the land cover in 2008, and the land cover products of 2000, 2004, 2012 and 2016 were obtained. The process was shown in Figure 2.

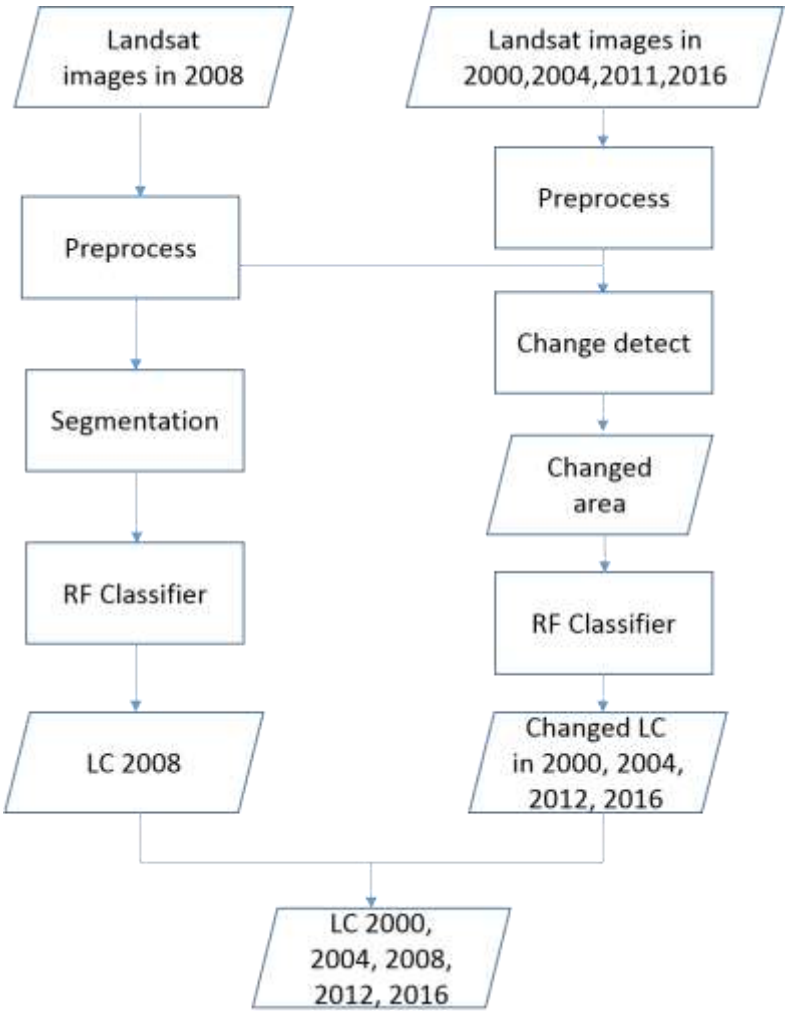

Figure 2. The flowchart.

3.1. Image segmentation

3.1.1 Mean shift segmentation method. Image segmentation is the foundation of the object-based classification [23]. The objective of image segmentation is to partition an image into spatially contiguous and homogeneous regions [24]. The segmented regions are viewed as image objects, which represent the core of object-based analysis. Generally, some parameters must be set for image segmentation, such as the spatial scale, bandwidth and shapes [25]. The mean shift algorithm has been widely used in image segmentation and identification tracking [26,27]. As a kernel density estimate method, the mean shift does not require prior knowledge of the number of segmentations and sets no limits on the segmented shape [28]. In this study, the mean shift method was used to segment the Landsat 5 image in 2008. The reflective bands with 30m resolution of the Landsat 5 images were segmented by mean shift. The Gaussian function was taken as the kernel function, and the bandwidths of the geometry space and color space were set to 10 and 8, respectively.

3.1.2 Object properties. The classification of objects requires more properties. In order to present the characteristics of the object, mean, variance, median, maximum, and minimum values of the objects on each band were counted, and the circumference and area of the object were also calculated. In addition, Normalized Difference Vegetation Index (NDVI) is a typical index of vegetation detection

and is also applied to this classification. So each object had a total of 8 characteristics to participate in the classification.

3.2. Random Forest classification

Random Forest is a supervised learning method that can be used to solve the problem of classification or regression [29]. It is made up of a combination of tree predictors so that each tree independently obtains the value of the random vector and has the same layout for each generated vector. Random forest is a collection of classifiers, which are structured as trees, each tree produces a vote according to the input. The random vector represents a set of random numbers that determine the structure of each tree. The RF classifier has been of interest in geo-mapping because of the small input parameters, the less sensitivity to noise and over fitting, and the ability to determine variable importance [30]. In FR, a random subset (image channels) of the variable are selected for each tree, and a random sample (with substitution) of the whole training samples are used to generate a single tree classification, and the remaining samples are used to verify the process. This process is referred to as bagging and the validation training areas provide an out-of-bag accuracy assessment for each tree. The RF classifier uses a voting system that votes the given class from all trees and forms the final classification map [31].

3.3. Change detect

The IR-MAD algorithm was used to detect the changed area, and then, the Spot5 images of the changed area were classified by the RF classifier. IR-MAD judged the unchanged pixels by iteratively calculating the chi-square distribution of the difference in the bi-temporal images [15, 32]. The IR-MAD linearly transformed the original images R and T to new images U and V based on the canonical correlation analysis (CCA) in Equation (1):

$$U = a^T R,\ V = b^T T, \tag{1}$$

Where U and V are the canonical correlation images, a^T and b^T are the transform matrixes and R and T are the bi-temporal images.

The bands of the canonical correlation images were referred to as the canonical variates. The canonical variates were arranged according to the correlations. If the correlation was relatively low, this pair of canonical variates had more change information. The differences in each pair of canonical variables were mutually uncorrelated.

According to the central limit theorem, the differences in the canonical variates approximately corresponded to a Gaussian distribution, and the sum of squares of the differences in the canonical variates corresponded to a chi-square distribution [15, 32]. The differences in the canonical variates and the weights of unchanged pixels were calculated by using Equations (2)–(4):

$$M_i = U_{N-i+1} - V_{N-i+1},\ i = 1,2,\ldots,N, \tag{2}$$

$$Z = \sum_{i=1}^{N} \left(\frac{M_i}{\sigma_{M_i}} \right)^2, \tag{3}$$

$$\Pr(no\ change) = 1 - P_{\chi^2;N}(Z), \tag{4}$$

where i is the band of the image, M_i is the difference in the variates, σ_{M_i} is the standard deviation of M_i, N is the total number of bands, $P_{\chi^2;N}(Z)$ is the χ^2 distributed with N degrees of freedom and $\Pr(no\ change)$ is the weight.

$\Pr(no\ change)$ is used to weigh each pixel. Then, Equations (1)–(4) are iterated until no significant changes observed in the canonical correlations. These pixels could then be determined as unchanged pixels if their chi-square distribution probability was lower than a threshold [15].

In this study, we calculated the chi-square images for 2004, 2008, 2016 based on the images from 2012. The threshold was slightly lower than 0.95, which was set by the developer, so some unchanged pixels were selected in the identified area. Although some extra unchanged pixels were selected, mostly changed pixels were chosen, so the omission error was reduced.

4. Result

4.1. Accuracy assessment

At present, the most common precision evaluation method is the confuse matrix method, that is, through the confusion matrix to calculate the various statistics and build the accuracy evaluation index, and finally give the accuracy of classification. The samples were selected by stratified random sampling. By referring to the Google Earth image for visual interpretation, the evaluation samples were collected to assess the classification accuracy. The confuse matrixes were constructed to calculate the overall accuracy, Kappa coefficient, user's accuracy, and producer's accuracy for2000, 2004, 2008, 2012, and 2016. The overall classification accuracy is expressed the consistent in probability between the classification results and test samples types for each random sample. The user's accuracy is the proportion of correctly-classified pixels with regard to all of the pixels that are classified as this class in the classified image. The producer's accuracy is the proportion of correctly-classified pixels with regard to all of the pixels of that ground truth class.

Table 2. The error matrix.

	2000		**2004**		**2008**		**2012**		**2016**	
	PA	**UA**	**PA**	**PA**	**UA**	**UA**	**PA**	**UA**	**UA**	**UA**
Forest	91.23	92.33	91.23	93.34	94.52	95.48	91.22	92.31	90.32	91.67
Grass	87.56	86.54	85.67	89.92	88.16	86.54	89.43	88.21	88.65	87.17
Dry Farmland	96.15	94.45	96.10	95.32	96.15	95.40	94.41	94.56	95.16	94.24
Paddy Field	94.27	90.12	94.48	93.67	94.43	91.34	94.27	89.28	94.34	87.54
Bare Land	95.87	94.56	96.34	95.66	95.36	95.65	95.32	95.29	95.43	95.16
Building	91.45	87.52	91.56	92.13	91.12	88.34	90.84	87.56	90.44	87.43
Water Body	95.13	95.89	90.43	95.66	96.23	95.91	95.43	95.47	95.32	95.18
Overall	93.02		93.11		94.72		94.12%		93.83	
Kappa	0.90		0.91		0.92		0.92		0.91	

The land cover in 2008 had the highest overall accuracy and Kappa coefficient, which were 94.72% and 0.92 respectively. The overall accuracies and Kappa coefficients were 93.02%, 93.11%, 94.12% and 93.83% and 0.90, 0.91, 0.92 and 0.91 for 2000, 2004, 2012, and 2016 respectively. Overall, the accuracy for 2008 was higher than other years. However, the difference was minor.

4.2. . Land cover and change

The land cover in the Xinlicheng Reservoir Basin has dramatically changed over the past 16 years. The sum of the areas of dry farmland, forests and impervious surfaces always exceeded 80% of the total study area during the 16 years. The most remarkable changes were the reduction in arable land. The arable land changed from 1117.54 km^2 to 1071.48 km^2 from 2000 to 2016, shrinking by 46 km^2.

The decrement of the arable land was mainly caused by Paddy Fields. The Paddy Fields decreased from 126.44 km^2 to 97.13 km^2 about 29.31km^2. The changes of the rest classes were far less than the arable land. The land cover areas in 2004 were different between other years because the decrement of water storage in Xinlicheng Reservoir in 2004. So the area of water body increased remarkably from 2000 to 2004 and increased from 2004 to 2008. The area of building was increased continually from 2000 to 2016, but the change was slow. From 2000 to 2016 only 4.70 km^2 about 0.24% of the total area. The areas and proportions of the classes are shown in Table 3.

Table 3. Areas of the classes for the five periods. (Unit: km^2)

	2000	**2004**	**2008**	**2012**	**2016**
Paddy Fields	126.44	151.31	115.71	113.54	97.13
Dry Farmland	991.10	961.99	987.56	959.91	974.35
Forests	573.18	576.29	574.29	580.38	581.87
Grass	48.24	79.25	54.23	80.75	79.78
Water Bodies	72.93	42.50	77.37	72.63	73.73
Building	129.50	129.98	132.25	133.85	134.21
Bare Land	0.30	0.38	0.29	0.64	0.64
Sum	1941.71	1941.71	1941.71	1941.71	1941.71

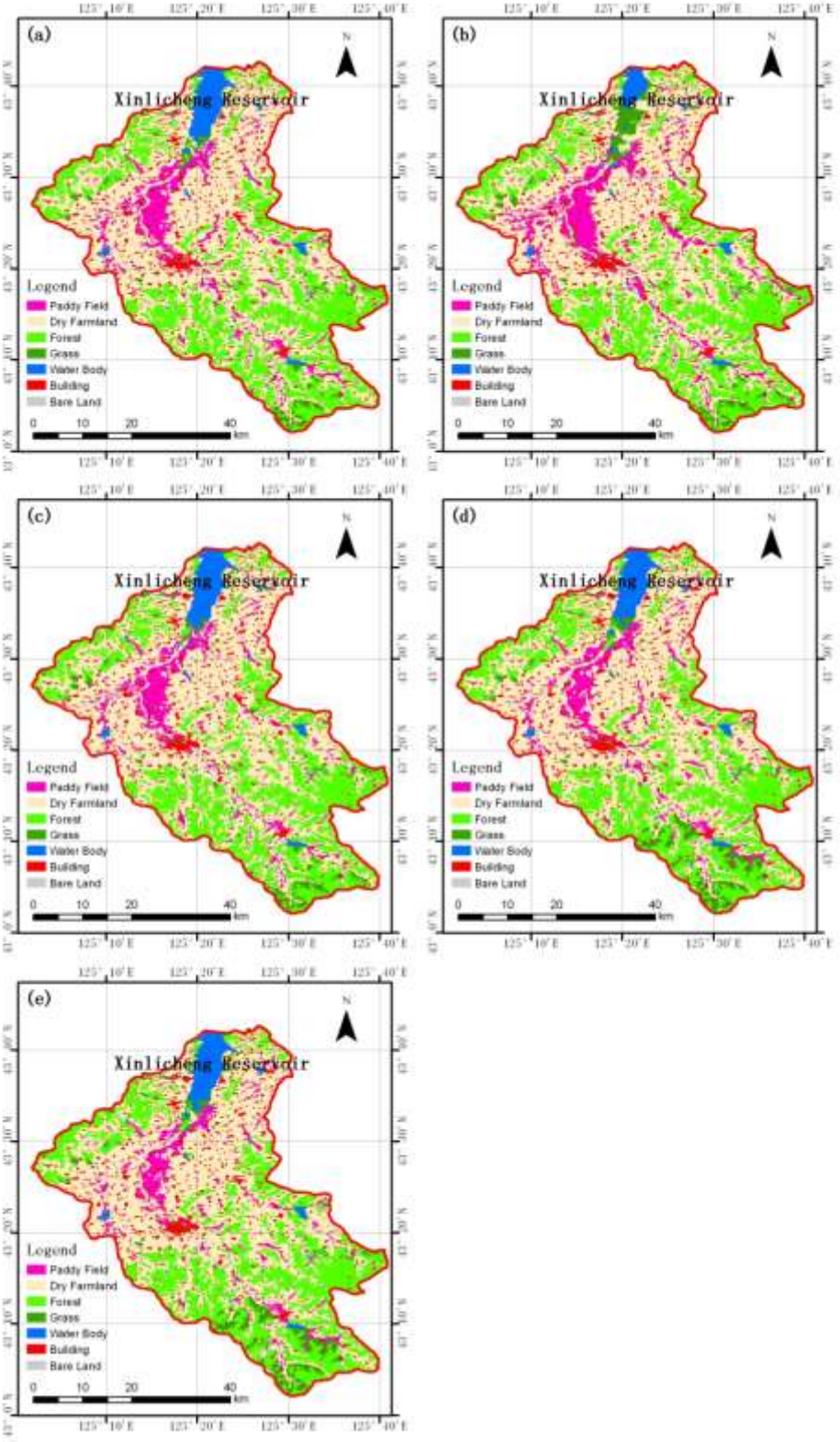

Figure 3. Land covers every 4 years from 2000 to 2016. From (a) to (e) corresponding the year from 2000 to 2016.

5. Discussion

The use of a consistent classification method is essential to ensure that the classification results at different times are comparable. The spectral characteristics of the different terrestrial order usually have some confusion or overlap, and are not always separated by a clear boundary. The transition between some classes, such as between bare and sparse grasslands and between wetlands and water bodies, is continuous. Classification errors usually occur near the differences between these classes, for their spectral similarity. The image has a unique Sun well-known geometric and weather characteristics. The same classifier is used to classify the images observed on each date. Happily, the boundary of unaltered land cover in the transitional area is difficult to identify stains. This type of discrepancy in boundary-adjacent areas can result in errors when comparing land covers between different periods. Generally, only a portion of the land cover in a region changes over a given period. If the identified change area is substantially larger than the actual change area, the updated effect is the same as the whole image of the classification. On the contrary, if the identified change area is a unique area, the error increase is omitted, and the unique area of the new area coverage product is the same as the basic product.

In this study, the software developer sets the threshold for changing the pixel to the inferred threshold, so the determined change area is slightly larger than actually changed region. This choice is to reduce omission errors. In general, the method of updating the change area reduces the computations required for classification and improves the consistency of land coverage between different periods.

6. Conclusion

Xinlicheng Reservoir Basin is an important ecological barrier and drinking water source for the residents in Changchun City. Rapid urbanization dramatically changes the local environment around Xinlicheng Reservoir Basin. Landsat images are suitable for the land use change caused by human impact. In order to obtain consistent land cover products, a hybrid classification method combining object-based classification and pre-classification alteration detection method was developed and applied to long-term multi-temporal Landsat images to obtain land cover change information. Object-based classification method can avoid the “salt and pepper” effect, and segment is the critical process in 0bject-based classification. As a kernel density estimate method, the mean shift method was used, which requires no prior knowledge of the number of segmentations and sets no limits on the object shape. Random forest (RF) classifier is less sensitivity to noise and over fitting and can determine variable importance. Pre-processed Landsat image in 2008 was segmented using the mean shift method, and then random forest (RF) classifier was used to classify the segmented objects. The changed areas in 2000, 2004, 2012, and 2016 were identified by comparing with the images in 2008 via the re–weighted multivariate alteration detection transformation method. The images in 2000, 2004, 2012 and 2016 were masked as changed areas and then were put into the RF classifier. Land cover maps for 2000, 2004, 2012, and 2016 were produced by combining the unchanged area in 2008 with the new classes of the changed areas in 2000, 2004, 2012 and 2016. In the study area, arable land remarkably decreased from 1117.54 km^2 to 1113.30 km^2, 1103.27 km^2, 1073.45 km^2 and 1071.48 km^2 in 2000, 2004, 2008, 2012 and 2016. Meanwhile, the building area continually increased from 129.50 km^2 to 129.98 km^2, 132.25 km^2, 133.85 km^2 and 134.20 km^2. Forest and grass all decreased in 2008 and then increased. The decrements were mainly caused by increasing of water storage in Xinlicheng Reservoir. Correspondingly, the water body area increased in 2008. Overall, the building increment area mainly from dry farmland and the sprawl speed is declining. According to the accuracy assessment, the overall accuracy of the land covers of the four periods are all greater than 93%. The accuracy assessment indicates that this hybrid method can produce consistent land cover datasets for a long time period.

Acknowledgments
This work was funded by the Research on Comprehensive Management Technology and Engineering Demonstration of Water Pollution in Yitong River Basin (2012ZX07201-001) fund, and Technical Research and Comprehensive Demonstration of Water Pollution Management and Water Quality Improvement in Yinma River Basin (2014ZX07201-011) fund.

References
[1] Du H, Wang D, Wang Y, Zhao X, Qin F, Jiang H and Cai Y 2016 Influences of land cover types, meteorological conditions, anthropogenic heat and urban area on surface urban heat island in the Yangtze River Delta Urban Agglomeration Science of The Total Environment 571 461-70
[2] Liu Q and Gong F 2013 Monitoring land use and land cover change: a combining approach of change detection to analyze urbanization in Shijiazhuang, China
[3] McCallum I, Obersteiner M, Nilsson S and Shvidenko A 2006 A spatial comparison of four satellite derived 1 km global land cover datasets International Journal of Applied Earth Observation and Geoinformation 8 246-55
[4] Saadat H, Adamowski J, Bonnell R, Sharifi F, Namdar M and Ale-Ebrahim S 2011 Land use and land cover classification over a large area in Iran based on single date analysis of satellite imagery ISPRS Journal of Photogrammetry and Remote Sensing 66 608-19
[5] Chen J, Chen J, Liao A, Cao X, Chen L, Chen X, He C, Han G, Peng S, Lu M, Zhang W, Tong X and Mills J 2015 Global land cover mapping at 30 m resolution: A POK-based operational approach Isprs Journal of Photogrammetry and Remote Sensing 103 7-27
[6] Friedl M A, Sulla-Menashe D, Tan B, Schneider A, Ramankutty N, Sibley A and Huang X 2010 MODIS Collection 5 global land cover: Algorithm refinements and characterization of new datasets Remote Sensing of Environment 114 168-82
[7] Hansen M C, Defries R S, Townshend J R G and Sohlberg R 2000 Global land cover classification at 1 km spatial resolution using a classification tree approach International Journal of Remote Sensing 21 1331-64
[8] Blaschke T 2010 Object based image analysis for remote sensing ISPRS Journal of Photogrammetry and Remote Sensing 65 2-16
[9] Blaschke T, Hay G J, Kelly M, Lang S, Hofmann P, Addink E, Queiroz Feitosa R, van der Meer F, van der Werff H, van Coillie F and Tiede D 2014 Geographic Object-Based Image Analysis – Towards a new paradigm ISPRS Journal of Photogrammetry and Remote Sensing 87 180-91
[10] Geneletti D and Gorte B G H 2003 A method for object-oriented land cover classification combining Landsat TM data and aerial photographs International Journal of Remote Sensing 24 1273-86
[11] Benz U C, Hofmann P, Willhauck G, Lingenfelder I and Heynen M 2004 Multi-resolution, object-oriented fuzzy analysis of remote sensing data for GIS-ready information ISPRS Journal of Photogrammetry and Remote Sensing 58 239-58
[12] Dorren L K A, Maier B and Seijmonsbergen A C 2003 Improved Landsat-based forest mapping in steep mountainous terrain using object-based classification Forest Ecology and Management 183 31-46
[13] Wang L, Sousa W P and Gong P 2004 Integration of object-based and pixel-based classification for mapping mangroves with IKONOS imagery International Journal of Remote Sensing 25 5655-68
[14] Vieira M A, Formaggio A R, Rennó C D, Atzberger C, Aguiar D A and Mello M P 2012 Object Based Image Analysis and Data Mining applied to a remotely sensed Landsat time-series to map sugarcane over large areas Remote Sensing of Environment 123 553-62
[15] Canty M J and Nielsen A A 2012 Linear and kernel methods for multivariate change detection Computers & Geosciences 38 107-14

[16] Nielsen A A and Canty M J 2010 Image and Signal Processing for Remote Sensing Xvi, ed L Bruzzone
[17] Sexton J O, Urban D L, Donohue M J and Song C 2013 Long-term land cover dynamics by multi-temporal classification across the Landsat-5 record Remote Sensing of Environment 128 246-58
[18] Hansen M C, Egorov A, Potapov P V, Stehman S V, Tyukavina A, Turubanova S A, Roy D P, Goetz S J, Loveland T R, Ju J, Kommareddy A, Kovalskyy V, Forsyth C and Bents T 2014 Monitoring conterminous United States (CONUS) land cover change with Web-Enabled Landsat Data (WELD) Remote Sensing of Environment 140 466-84
[19] Gong P, Wang J, Yu L, Zhao Y, Zhao Y, Liang L, Niu Z, Huang X, Fu H, Liu S, Li C, Li X, Fu W, Liu C, Xu Y, Wang X, Cheng Q, Hu L, Yao W, Zhang H, Zhu P, Zhao Z, Zhang H, Zheng Y, Ji L, Zhang Y, Chen H, Yan A, Guo J, Yu L, Wang L, Liu X, Shi T, Zhu M, Chen Y, Yang G, Tang P, Xu B, Giri C, Clinton N, Zhu Z, Chen J and Chen J 2013 Finer resolution observation and monitoring of global land cover: first mapping results with Landsat TM and ETM+ data International Journal of Remote Sensing 34 2607-54
[20] Yang L, Huang C, Homer C G, Wylie B K and Coan M J 2003 An approach for mapping large-area impervious surfaces: synergistic use of Landsat-7 ETM+ and high spatial resolution imagery Canadian Journal of Remote Sensing 29 230-40
[21] Liu J, Kuang W, Zhang Z, Xu X, Qin Y, Ning J, Zhou W, Zhang S, Li R, Yan C, Wu S, Shi X, Jiang N, Yu D, Pan X and Chi W 2014 Spatiotemporal characteristics, patterns, and causes of land-use changes in China since the late 1980s Journal of Geographical Sciences 24 195-210
[22] Gao F, Masek J, Schwaller M and Hall F 2006 On the blending of the Landsat and MODIS surface reflectance: predicting daily Landsat surface reflectance IEEE Transactions on Geoscience & Remote Sensing 44 2207-18
[23] Johnson B and Xie Z 2011 Unsupervised image segmentation evaluation and refinement using a multi-scale approach ISPRS Journal of Photogrammetry and Remote Sensing 66 473-83
[24] Myint S W, Gober P, Brazel A, Grossman-Clarke S and Weng Q 2011 Per-pixel vs. object-based classification of urban land cover extraction using high spatial resolution imagery
[25] Yu W, Zhou W, Qian Y and Yan J 2016 A new approach for land cover classification and change analysis: Integrating backdating and an object-based method Remote Sensing of Environment 177 37-47
[26] Fukunaga K and Hostetler L 1975 The estimation of the gradient of a density function, with applications in pattern recognition Information Theory, IEEE Transactions on 21 32-40
[27] Cheng Y 1995 Mean shift, mode seeking, and clustering Pattern Analysis and Machine Intelligence, IEEE Transactions on 17 790-9
[28] Comaniciu D and Meer P 2002 Mean shift: a robust approach toward feature space analysis Pattern Analysis and Machine Intelligence, IEEE Transactions on 24 603-19
[29] Shiraishi T, Motohka T, Thapa R B, Watanabe M and Shimada M 2014 Comparative Assessment of Supervised Classifiers for Land Use–Land Cover Classification in a Tropical Region Using Time-Series PALSAR Mosaic Data IEEE Journal of Selected Topics in Applied Earth Observations and Remote Sensing 7 1186-99
[30] Yu L, Wang J and Gong P 2013 Improving 30 m global land-cover map FROM-GLC with time series MODIS and auxiliary data sets: a segmentation-based approach International Journal of Remote Sensing 34 5851-67
[31] Pelletier C, Valero S, Inglada J, Champion N and Dedieu G 2016 Assessing the robustness of Random Forests to map land cover with high resolution satellite image time series over large areas Remote Sensing of Environment 187 156-68
[32] Canty M J and Nielsen A A 2008 Automatic radiometric normalization of multitemporal satellite imagery with the iteratively re-weighted MAD transformation Remote Sensing of Environment 112 1025-36